Surface Science xxx (2015) xxx–xxx

Contents lists available at ScienceDirect

Surface Science

journal homepage: www.elsevier.com/locate/susc

Real-time observation of graphene oxidation on Pt(111) by low-energy electron microscopy

Viktor Johánek [a,b,*], Gregory W. Cushing [a], Jason K. Navin [a], Ian Harrison [a]

[a] Department of Chemistry, University of Virginia, Charlottesville, VA 22904-4319, United States
[b] Department of Surface and Plasma Science, Charles University in Prague, V Holesovickach 2, 180 00 Prague 8, Czech Republic

ARTICLE INFO

Article history:
Received 3 June 2015
Accepted 26 August 2015
Available online xxxx

Keywords:
Graphene
Platinum
Oxidation
Low-energy electron microscopy
Intercalation

ABSTRACT

A monolayer of graphene was prepared by thermal decomposition of ethylene gas on Pt(111). The graphene can be readily removed by dosing O_2 at pressures in 10^{-8} mbar range and surface temperatures (T_s) near 1000 K. Residual gas analysis during the oxygen treatment of graphene layer detected CO to be the only formed product. The oxidation process has been continuously imaged by Low-energy Electron Microscope (LEEM) operated in mirror-electron mode. LEEM observations revealed that the oxidation of graphene on Pt(111) occurs simultaneously at the outer island perimeter and in the interior of the graphene island. Symmetric hexagonal pits were observed to form continuously within graphene sheets, the pits proceeded isotropically. The etch rate was determined to be equal for both modes and independent of the surface environment with the exception of areas above Pt step edges. The pit growth rate at constant oxygen pressure was found to increase exponentially with respect to temperature over the investigated T_s range of 927–1014 K, yielding an apparent activation energy of 479 kJ/mol.

1. Introduction

Graphene is an sp^2-hybridized C monolayer with extraordinary physical [1], chemical [2], and electronic [3,4] properties. Its growth and reactivity have been most frequently studied on metals, primarily on hexagonal surfaces, e.g. on (111) face of fcc metals (such as Pt, Rh, Ir, Pd, Cu, Au, Ni) or on (0001) face of hcp metals (Ru, Re, Co) [5,6]. The properties of the substrate determine the metal–graphene interaction strength (ranging from weak van der Waals physisorption to strong bonding through chemisorption), level of graphene corrugation, its mean distance from the substrate, etc. [7], having numerous implications for the chemical and physical properties of the graphene adlayer. For instance, controlling the level of defects such as vacancies, wrinkles, or boundaries between rotational domains in a sheet of graphene has become an important factor for engineering graphene tensile strength. A potential role of such defects in the reactivity or, in turn, chemical stability of graphene also remains one of the key issues in this greatly expanding field. The detailed knowledge of the way graphitic carbon reacts with oxygen is important, e.g., in reactivation of catalysts poisoned with carbon [8], combustion chemistry [9], production of graphene oxide [10], graphene functionalization [11], etc. [12,13].

It has been demonstrated [14–17] that the mechanisms by which oxygen interacts with graphitic structures can generally can proceed via two main pathways—oxidation of terminal carbon atoms at the outer edges of graphite/graphene layers and oxidation of carbon atoms within their interiors. As a result of the latter process, creation of holes or hollow structures on HOPG is observed, both layer by layer and across several layers [17], depending on the reaction conditions. Very uniform distribution of pit sizes up to a certain temperature limit has been attributed to the simultaneous pit formation on naturally occurring point defects (mainly vacancies) on the surface [14,15,18]. At higher temperatures (>1148 K according to [14]) pit formation in HOPG layers occurs via etching at both defected and basal plane carbon atoms resulting in significantly broader pit diameter distribution. It has been suggested that atomic oxygen is responsible for the abstraction of the basal plane carbon [19].

The oxidation of other graphitic structures such as monolayer or multilayer graphene on metals follows the similar scheme in terms of the above two etching modes but exact mechanisms and corresponding etching conditions differ depending on the metal type and surface plane orientation. E.g., on Ru(0001) oxidation proceeds via two sequential processes involving 1) oxygen interaction with the carbon released from the graphene edges and diffusing over the metal surface as carbon ad-atoms, and 2) oxygen penetration underneath the graphene, weakening its interaction with the substrate and attacking it to form highly disintegrated ("cracked") structures, while on Ir(111) the intercalated oxygen tends to create irregular holes across the graphene islands [16,20].

Since most of the recent literature dealing with microscopic insight into graphene oxidation is based on experimental techniques which are typically too slow to capture it directly, a reliable kinetic analysis of this process is difficult. In this study we present a real-time in situ

* Corresponding author. Tel.: +420 22191 2333; fax: +420 22191 2297.
E-mail address: viktor.johanek@mff.cuni.cz (V. Johánek).

http://dx.doi.org/10.1016/j.susc.2015.08.042
0039-6028/

imaging of graphene oxidation at temperatures near 1000 K on the (111) face of platinum. The reaction kinetics is quantified and the LEEM observations are related to findings on other similar systems.

2. Experimental

The experiments were performed using Low-energy Electron Microscope (LEEM) from Specs-GmbH (model FE-LEEM P90) that was housed in an ultrahigh vacuum (UHV) chamber with a base pressure $<1 \times 10^{-10}$ mbar. The Specs LEEM is a commercial version of Ruud Tromp's LEEM II [21]. A 99.999% purity Pt single crystal sample of approximately 10 mm diameter and 1.5 mm thickness cut into a top-hat shape that could be fitted into the LEEM's Mo sample holder was obtained from Surface Preparation Laboratory, The Netherlands. The 5 mm diameter top face of the sample was polished and oriented to within 0.1° of the Pt(111) surface. A K-type thermocouple attached to the backside of the sample, calibrated against a pyrometer (Pyrolaser PL905) for temperatures above 900 K, was used to monitor the Pt(111) surface temperature. The Pt(111) surface was cleaned by cycles of Ar^+ ion sputtering at 800 K followed by annealing to 1200 K. The sample was exposed to a 3×10^{-8} mbar O_2 atmosphere to remove C contaminants followed by a brief flashing to 1200 K. The Pt(111) surface was imaged under reaction conditions with the LEEM [21] operating in mirror-electron mode (MEM) with an image acquisition rate of 2 frames/s, an image exposure time of 200 ms per frame, and a typical field-of-view (FOV) diameter 5–10 μm. In MEM, the surface is electrically reverse biased such that the incident electron beam is returned from the surface retarding field just before actually striking the physical surface. In this way, possibilities for electron-induced surface chemistry are minimized, if not eliminated entirely. Contrast in MEM images arises from variations in the local work function and surface topology that modulate the surface retarding field [22,23].

Graphene layers were grown by thermal decomposition of ethylene gas (CP grade, 99.5%, Matheson Tri-Gas) which was introduced at room temperature via a directed doser onto the Pt(111) sample through a 2 mm inner dia., 150 mm long tube from a distance of 30 mm at 18° glancing incidence angle from the surface plane to enhance the molecular impingement rate at the sample surface. For this geometry, the directed ethylene gas flux at the sample is calculated to enhance the net flux striking the surface 4-fold as compared to the ambient flux [24]. The standard local ethylene dosing pressure (i.e., pressure at sample surface calculated to account for the doser enhancement factor) during CVD in LEEM experiments was 4×10^{-8} mbar. The deposition was stopped when the relative graphene coverage reached a typical value of 70%. For oxidation experiments the same dosing setup was used with typical pressures of 2×10^{-8} mbar of pure oxygen (99.999%, Matheson Tri-Gas) at the sample surface.

3. Results and discussion

Carbon produced by thermal decomposition of ethylene gas ($T_g = 300$ K) at surface temperatures near $T_s = 1000$ K has been shown to produce graphene, i.e. a flat single C(0001) layer [25–27]. Single oriented graphene islands were observed to grow to diameters ≥10 μm, despite the presence of many Pt(111) steps underneath [25]. Coexistence of multiple orientations of graphene islands was identified using LEEM operated in localized microdiffraction (μLEED) mode, majority of them being $(\sqrt{7} \times \sqrt{7})$R19.1° and $(\sqrt{19} \times \sqrt{19})$R23.4° superstructures with respect to Pt lattice [25]. When the incident energy of the primary electrons in LEEM is set for MEM a layer of graphene on platinum can be distinguished by an image contrast between the Pt substrate and subsequent graphene layers [28]. Moreover, MEM exhibits sharp contrast at the graphene islands edges where the local electronic structure/work function perimeter is likely most perturbed. Contrast lines are also observed at boundaries between two adjacent islands of mismatched orientation with respect to the underlying Pt(111) surface (see, e.g., dotted line in Fig. 1). All the islands appeared continuous with no visible holes or other defects on the scale of our LEEM resolution of about 5 nm.

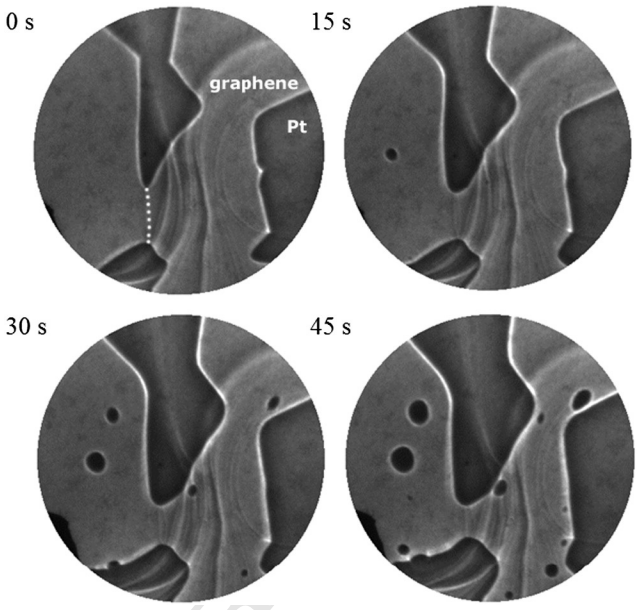

Fig. 1. A sequence of time-labeled LEEM images (10 μm field of view) of graphene oxidation on Pt(111) at $T_s = 986$ K, $P_{O2} = 2 \times 10^{-8}$ mbar. Highlighted is the boundary between two graphene domains with different lattice orientations (dotted line in top left image).

Fig. 1 shows the sequence of oxidizing a single discontinuous layer of graphene in 2×10^{-8} mbar of oxygen at $T_s = 986$ K. The LEEM snapshots were selected from a movie over a time period of 45 s. As could be expected, the sheets of graphene shrink due to the oxygen etching of their outer edges. Moreover, pits are seen to form in the interior of graphene during oxygen treatment similar to pits reported on HOPG [14]. No additional pits were observed to form after the graphene layer was removed which supports the above claim that no additional layers of graphene were produced by ethylene CVD. Residual gas analysis during the oxygen treatment found that carbon monoxide is the only formed product, no CO_2 above the background level was detected. A removal of carbon via its diffusion into the platinum bulk can be ruled out under our temperature and pressure conditions [29,30].

The pits in Fig. 1 are observed as round holes due to an adjustment of the objective lens focusing more on the surface than the graphene sheet. Adjusting the electron beam such that the focus is on the graphene sheet, it is observed that the pits are hexagonally shaped as seen in Fig. 2. The hexagonal pits are observed to have a regular interior angle of 120°. The pits advance isotropically in the presence of O_2. The

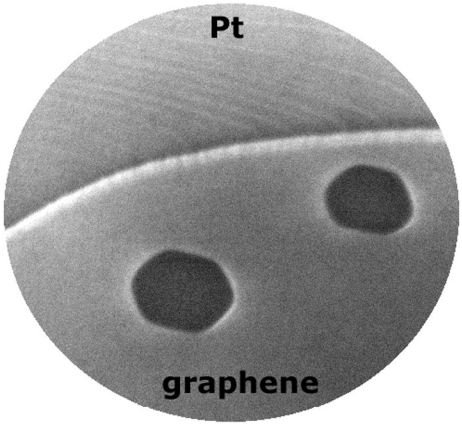

Fig. 2. Hexagonally shaped pits are observed to form in the interior of the graphene island. $T_s = 986$ K, imaging FOV diameter is 5 μm.

Please cite this article as: V. Johánek, et al., Real-time observation of graphene oxidation on Pt(111) by low-energy electron microscopy, Surf. Sci. (2015), http://dx.doi.org/10.1016/j.susc.2015.08.042

symmetry of the pit is presumed to reflect the internal unit structure of graphene being a 6-fold symmetric 6 C-membered ring. Establishment of such structures, not observed on graphene supported by Ir(111) or Ru(0001) [16,20], is probably owing to the fact that graphene is well decoupled from the Pt(111) surface [28,31,32] and that the surface temperature is high enough to allow carbon atoms to easily diffuse along the edges of graphene [33], keeping a minimum-energy equilibrium shape.

Oxygen has been suggested to intercalate between the basal planes of graphite [34], as well as on several graphene/transition metal systems—e.g., a similar mechanism in graphene oxidation on Ru(0001) has been recently described [16,20,35]; it has also been shown that intercalated oxygen is responsible for hole formation on Ir(111) [16]. On the contrary, a direct pit formation by oxygen penetration through graphene layer is essentially impossible at low pressures as it was demonstrated [28] that structurally coherent graphene sheet represents very effective diffusion barrier. Very recently, oxygen penetration through full graphene monolayer has been reported on Ru(0001) [36], resulting in decoupling of the graphene overlayer from the metal surface; however, much higher pressures close to ambient were required to allow such mechanism. A cartoon depiction of the intercalation mechanism is shown in Fig. 3.

The spacing between the graphene sheet and the Pt(111) surface is known to be some 3.70 ± 0.05 Å [37], which is even greater than the spacing between graphite planes in bulk graphite of 3.35 Å [38]. A NEXAFS study of several graphene/transition metal systems indicated that graphene is only weakly bound to Pt(111) in comparison to most other metals [39]. It was also shown by He/Ar atom scattering experiment [31], LEEM [28], and scanning tunneling microscopy measurement with density functional theory calculation [32] that graphene is well decoupled from the Pt(111) surface. Such a large gap between the graphene over-layer and the Pt substrate would allow oxygen to readily intercalate below the graphene sheet as indicated by other LEEM studies of graphene oxidation on Ir(111) [16], by photoelectron spectroscopy [40,41], and by STM [41]. The intercalation is even allowed on stronger binding substrates such as Ru(0001) where oxygen can break strong coupling between graphene and the metal, but this step requires non-negligible energy and thus competes with the etching process at higher temperatures [20].

The growth rates of the pits were measured between T_s = 927–1014 K. The edge velocity can be determined from $v = dA / Pdt$ where A is the pit area and P is the perimeter. The growth rates were found to increase exponentially with an increase in T_s. An Arrhenius fit to the pit growth rate with respect to the surface temperature (Fig. 4) yields and activation energy of $E_a = 479 \pm 29$ kJ/mol and pre-exponential factor of $2.7 \times 10^{17 \pm 1}$ (s^{-1}). Our activation energy measured for oxidation of graphene on Pt(111) is much higher than for carbon combustion reactions [42] and graphite oxidation [15] (E_a of lateral etching of HOPG reported in recent literature spans 127–168 kJ/mol [14,17,18,43]) which indicates a substantial barrier for CO production or any of the preceding reactions steps. It should be noted, that unlike in our experiment the works cited above involve oxidation in ambient or near-ambient oxygen partial pressures, needed to achieve a reasonable

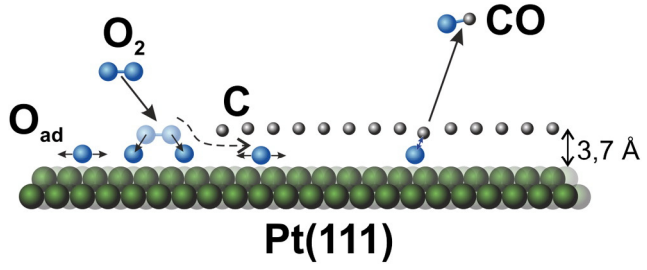

Fig. 3. Cartoon depiction of the mechanism by which oxygen can intercalate between the graphene sheet and the Pt(111) surface and oxidize the graphene.

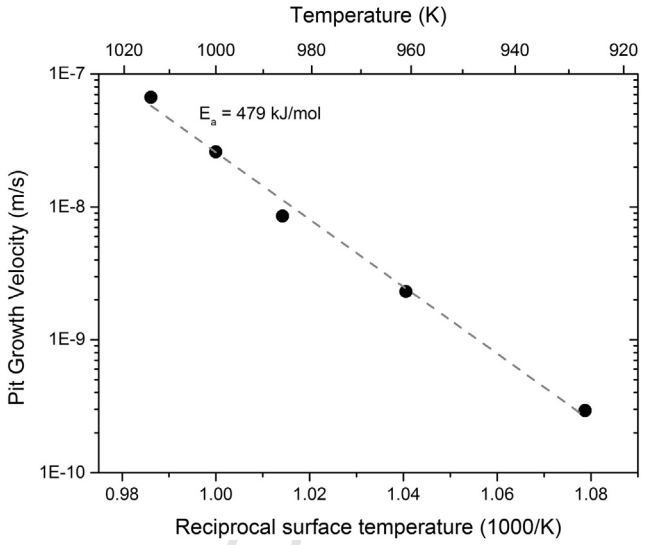

Fig. 4. Graphene pit growth rate (measured in terms of edge velocity) by oxygen etching over a surface temperature range of T_s = 927–1014 K (solid points) and local oxygen pressure $P_{O2} = 2 \times 10^{-8}$ mbar. The dashed line is an Arrhenius fit to the etching rate.

etching effect since the well-ordered HOPG is highly resistant to molecular oxygen and the O_2 dissociation rate is very low on the basal plane of graphite [18,44]. Nevertheless, we suppose that the comparison of activation energies is sufficiently relevant as the molecular oxygen is just a spectator in the etching mechanism and it is primarily the surface occupation with more strongly bound atomic oxygen that affects the reaction kinetics.

Most likely the rate limiting step is the weakening and a subsequent destruction of the C—C sp^2 bonds adjacent to the oxygen atom [44] preceding the formation of the covalent C—O bond. The required activation energy for this process is supposedly higher than on graphite because of the larger spatial separation between O_{ad} and carbon atoms of graphene on Pt(111) (d_{Pt-O} = 2.01 Å [45] for the most preferred 3-fold hollow site, d_{Pt-C} = 3.70 Å [37], yielding $d_{C-O} \geq 1.69$ Å) as compared to the most preferred bridge site on HOPG (d_{C-O} = 1.43 Å [44]). Moreover, the oxygen affinity to creating a covalent bond with carbon is further suppressed by the relatively strong [45,46] existing Pt—O bond.

The pre-exponential factor for graphene oxidation on Pt(111) is also found to be considerably larger than that of HOPG with a typical value of 10^{10}–10^{12} (s^{-1}) [14,17,18]. Such a large difference in pre-exponential factor would further indicate that direct reaction of O_2 on the graphene layer on Pt(111) does not occur, but rather O_2 is first dissociated on the Pt surface before reaction with a carbon ad-atom via Langmuir–Hinshelwood mechanism and its value reflects much higher O_2 sticking and dissociation probability on Pt [47,48] than on pure graphite [18,44].

We found no discernible difference in the etching rate of the outside edges as compared to the inner (pit) etching within the investigated temperature range; furthermore, the O etching rate was found to be independent of the coverage of graphene, indicating that CO production from graphene oxidation on Pt(111) is determined neither by oxygen surface diffusion, nor by O_2 impingement rate, but rather is limited by another process. According to the previous discussion of the activation energy it is presumably the carbon–oxygen bond formation which governs the overall etching rate.

It is suggested that graphite etching investigations using STM can under estimate the monolayer oxidation activation energy owning to our real-time observation of graphene oxidation on Pt(111) that the pits are not initialized at the same time, but rather are continuously forming during the oxidation process [14,17]. Hence, it would rather appear to be more appropriate to consider activation energies determined from such static methods as a lower bound value to the real activation energy of graphite etching. Since there is only a limited amount of

Please cite this article as: V. Johánek, et al., Real-time observation of graphene oxidation on Pt(111) by low-energy electron microscopy, Surf. Sci. (2015), http://dx.doi.org/10.1016/j.susc.2015.08.042

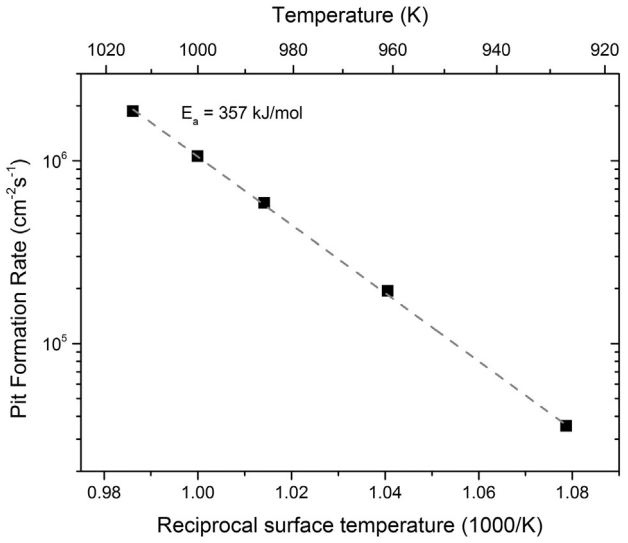

Fig. 5. Pit formation rate on graphene/Pt(111) during oxygen etching over a surface temperature range of $T_c = 927–1014$ K and local oxygen pressure $P_{O2} = 2 \times 10^{-8}$ mbar.

surface defects in each carbon layer, simultaneous etching at both defected and basal plane carbon atoms results in significantly broader pit diameter distribution, in accord with our observations. No correlation was found between the location of pit origins and boundaries between islands of different orientation (such as in Fig. 1). However, the occurrence of the pits was detected to be slightly more frequent directly above the platinum step edges than above flat Pt terraces.

The above observations suggest that the initial step of pit creation is, at least in the studied temperature range, apparently a stochastic process driven by local temperature-induced fluctuations of graphene structure [33,49] which can be further enhanced by the presence of dissociated oxygen. The observed slight preference for etching near step edges is likely the result of the localization of O atoms in their vicinity due to the stronger interaction of oxygen with less coordinated Pt atoms [50].

The stochastic nature of the initial attack of inner carbon atoms by oxygen is well documented in Fig. 5 where the pit formation rate within graphene (expressed in terms of number of new pits created per unit surface area per time) is plotted versus reciprocal surface temperature. The formation rate scales exponentially with temperature as could be expected for a random process driven by thermal fluctuations of carbon atoms within the graphene lattice. The apparent activation energy of the pit formation 357 ± 17 kJ/mol can be compared to the energy required to create a monovacancy defect on the graphite surface (193 kJ/mol in [14]). In accord with the above discussion of the etch velocity, we ascribe the higher energy required on the Pt/graphene system to the larger distance between C atoms and O ad-atoms as well as to the extra energy required to break the previously established Pt—O_{ad} bond.

4. Conclusions

Large graphene 2-dimensional islands (exceeding 10 μm diameter at 1014 K) were prepared by exposure of Pt(111) single-crystal surface to ethylene under CVD conditions at ~1000 K. Exposure of such surface to oxygen leads to complete graphene removal via reaction to carbon monoxide, and its immediate desorption. It was demonstrated by direct imaging that graphene on platinum can be oxidized near 1000 K not only by oxidation of terminal carbons at the outer edges of graphene sheets but also in their interiors. The pits are created via an intercalated oxygen mechanism in which oxygen atoms can travel underneath the graphene overlayer and attack the internal carbon atoms. The pits advance isotropically in the presence of O_2, reflecting the 6-fold symmetry of graphene elementary cell. In contrast to some reports on HOPG and graphene supported on stronger interacting metal substrates where pit etching mode is claimed to occur at presumed irregularities that are present within the C-layers (C-atom vacancies, wrinkles, rotational domain boundaries, etc.), the creation of pits in high-quality graphene on Pt(111) near 1000 K is likely a purely stochastic process. Nevertheless, a partial spatial correlation between the pit origins and the local structure of the Pt substrate has been found. It has been suggested analogously that the variation in pit diameter observed by others on HOPG after oxidation at high temperatures is an evidence for continuous pit formation rather than variations in etch kinetics. The activation energy 479 kJ/mol for graphene etching is surprisingly large in comparison to HOPG. It is suggested that the rate-limiting step in graphene oxidation on Pt(111) near 1000 K is the weakening of the regular C—C sp^2 bonds adjacent to oxygen atoms diffusing over the carbon-covered platinum, which is a prerequisite for C—O bond formation via which the carbon is removed from the surface.

Acknowledgment

This work was supported by National Science Foundation Grants DMR-0421152 and CHE-0718657, and a University of Virginia NanoStar Seed Fund. V.J. acknowledges the support by GAUK grant #339311.

References

[1] A.K. Geim, Science 324 (2009) 1530.
[2] M.J. Allen, V.C. Tung, R.B. Kaner, Chem. Rev. 110 (2010) 132.
[3] A.H. Castro Neto, F. Guinea, N.M.R. Peres, K.S. Novoselov, A.K. Geim, Rev. Mod. Phys. 81 (2009) 109.
[4] A.K. Geim, K.S. Novoselov, Nat. Mater. 6 (2007) 183.
[5] J. Wintterlin, M.L. Bocquet, Surf. Sci. 603 (2009) 1841.
[6] R. Munoz, C. Gomez-Aleixandre, Chem. Vap. Depos. 19 (2013) 297.
[7] K.V. Emtsev, A. Bostwick, K. Horn, J. Jobst, G.L. Kellogg, L. Ley, J.L. McChesney, T. Ohta, S.A. Reshanov, J. Rohrl, E. Rotenberg, A.K. Schmid, D. Waldmann, H.B. Weber, T. Seyller, Nat. Mater. 8 (2009) 203.
[8] C.J. Weststrate, A.C. Kizilkaya, E.T.R. Rossen, M.W.G.M. Verhoeven, I.M. Ciobica, A.M. Saib, J.W. Niemantsverdriet, J. Phys. Chem. C 116 (2012) 11575.
[9] R. Whitesides, A.C. Kollias, D. Domin, W.A. Lester, M. Frenklach, Proc. Combust. Inst. 31 (2007) 539.
[10] S.Z. Liu, W.C. Peng, H.Q. Sun, S.B. Wang, Nanoscale 6 (2014) 766.
[11] T. Kuila, S. Bose, A.K. Mishra, P. Khanra, N.H. Kim, J.H. Lee, Prog. Mater. Sci. 57 (2012) 1061.
[12] V. Singh, D. Joung, L. Zhai, S. Das, S.I. Khondaker, S. Seal, Prog. Mater. Sci. 56 (2011) 1178.
[13] C. Soldano, A. Mahmood, E. Dujardin, Carbon 48 (2010) 2127.
[14] J.R. Hahn, Carbon 43 (2005) 1506.
[15] J.R. Hahn, H. Kang, S.M. Lee, Y.H. Lee, J. Phys. Chem. B 103 (1999) 9944.
[16] E. Starodub, N.C. Bartelt, K.F. McCarty, J. Phys. Chem. C 114 (2010) 5134.
[17] F. Stevens, L.A. Kolodny, T.P. Beebe, J. Phys. Chem. B 102 (1998) 10799.
[18] X. Chu, L.D. Schmidt, Surf. Sci. 268 (1992) 325.
[19] R.T. Yang, K.L. Yang, Carbon 23 (1985) 537.
[20] P. Sutter, J.T. Sadowski, E.A. Sutter, J. Am. Chem. Soc. 132 (2010) 8175.
[21] R.M. Tromp, IBM J. Res. Dev. 44 (2000) 503.
[22] M.E. Barnett, W.C. Nixon, J. Sci. Instrum. 44 (1967) 893.
[23] T. Shimakura, Y. Takahashi, M. Sugaya, T. Ohnishi, M. Hasegawa, H. Ohta, Microelectron. Eng. 85 (2008) 1811.
[24] H. Pauly, Other low-energy beam sources, in: G. Scoles (Ed.), Atomic and Molecular Beam Methods, Oxford Univ. Press, New York 1988, p. 83.
[25] G.W. Cushing, V. Johánek, J.K. Navin, I. Harrison, J. Phys. Chem. C 119 (2015) 4759.
[26] K.M. DeWitt, L. Valadez, H.L. Abbott, K.W. Kolasinski, I. Harrison, J. Phys. Chem. B 110 (2006) 6705.
[27] K.M. DeWitt, L. Valadez, H.L. Abbott, K.W. Kolasinski, I. Harrison, J. Phys. Chem. B 110 (2006) 6714.
[28] P. Sutter, J.T. Sadowski, E. Sutter, Phys. Rev. B 80 (2009), 245411.
[29] G.W. Cushing, J.K. Navin, S.B. Donald, L. Valadez, V. Johanek, I. Harrison, J. Phys. Chem. C 114 (2010) 17222.
[30] J.C. Hamilton, J.M. Blakely, Surf. Sci. 91 (1980) 199.
[31] Y. Yamada, C. Sugawara, Y. Satake, Y. Yokoyama, R. Okada, T. Nakayama, M. Sasaki, T. Kondo, J. Oh, J. Nakamura, W.W. Hayes, J. Phys. Condens. Matter 22 (2010), 304010.
[32] M. Gao, Y. Pan, C.D. Zhang, H. Hu, R. Yang, H.L. Lu, J.M. Cai, S.X. Du, F. Liu, H.J. Gao, Appl. Phys. Lett. 96 (2010), 053109.
[33] C.O. Girit, J.C. Meyer, R. Erni, M.D. Rossell, C. Kisielowski, L. Yang, C.H. Park, M.F. Crommie, M.L. Cohen, S.G. Louie, A. Zettl, Science 323 (2009) 1705.
[34] Z.J. Pan, R.T. Yang, Ind. Eng. Chem. Res. 31 (1992) 2675.
[35] Y. Cui, Q. Fu, H. Zhang, D.L. Tan, X.H. Bao, J. Phys. Chem. C 113 (2009) 20365.
[36] A. Dong, Q. Fu, M. Wei, Y. Liu, Y. Ning, F. Yang, H. Bluhm, X. Bao, Surf. Sci. 634 (2015) 37.
[37] Z.P. Hu, D.F. Ogletree, M.A. Vanhove, G.A. Somorjai, Surf. Sci. 180 (1987) 433.

[38] H.O. Pierson, Handbook of Carbon, Graphite, Diamond and Fullerenes, Noyes Publications, Park Ridge, 1993.
[39] A.B. Preobrajenski, M.L. Ng, A.S. Vinogradov, N. Martensson, Phys. Rev. B 78 (2008), 073401.
[40] R. Larciprete, S. Ulstrup, P. Lacovig, M. Dalmiglio, M. Bianchi, F. Mazzola, L. Hornekaer, F. Orlando, A. Baraldi, P. Hofmann, S. Lizzit, ACS Nano 6 (2012) 9551.
[41] E. Granas, J. Knudsen, U.A. Schroder, T. Gerber, C. Busse, M.A. Arman, K. Schulte, J.N. Andersen, T. Michely, ACS Nano 6 (2012) 9951.
[42] Z.Y. Du, A.F. Sarofim, J.P. Longwell, C.A. Mims, Energy Fuel 5 (1991) 214.
[43] X. Chu, L.D. Schmidt, Carbon 29 (1991) 1251.
[44] D. Lamoen, B.N.J. Persson, J. Chem. Phys. 108 (1998) 3332.
[45] T. Jacob, R.P. Muller, W.A. Goddard, J. Phys. Chem. B 107 (2003) 9465.
[46] P. Legare, Surf. Sci. 580 (2005) 137.
[47] J.L. Gland, V.N. Korchak, Surf. Sci. 75 (1978) 733.
[48] T. Zambelli, J.V. Barth, J. Wintterlin, G. Ertl, Nature 390 (1997) 495.
[49] L. Liu, S.M. Ryu, M.R. Tomasik, E. Stolyarova, N. Jung, M.S. Hybertsen, M.L. Steigerwald, L.E. Brus, G.W. Flynn, Nano Lett. 8 (2008) 1965.
[50] P. Gambardella, Z. Sljivancanin, B. Hammer, M. Blanc, K. Kuhnke, K. Kern, Phys. Rev. Lett. 87 (2001), 056103.

Please cite this article as: V. Johánek, et al., Real-time observation of graphene oxidation on Pt(111) by low-energy electron microscopy, Surf. Sci. (2015), http://dx.doi.org/10.1016/j.susc.2015.08.042